Flotillin-1 palmitoylation is essential for its stability and subsequent tumor promoting capabilities

Linda deGraffenried (degraffenried@austin.utexas.edu)
University of Texas at Austin
Bryan Mcclellan
University of Texas at Ausin https://orcid.org/0000-0003-2760-3939
Crystal Wilson
Andrew Brenner
Christopher Jolly

Article

Keywords: Palmitoylation, Breast Cancer, Flotillin-1, Tumor Metastasis, Translational Research

Posted Date: October 29th, 2023

DOI: https://doi.org/10.21203/rs.3.rs-3487749/v1

Additional Declarations: There is **NO** conflict of interest to disclose.

Abstract

Flotillin-1 contributes to invasion and metastasis in triple negative breast cancer (TNBC) and is modified post-translationally through palmitoylation. Palmitoylation, the process of conjugating palmitoyl-CoA to proteins, plays an essential role in protein stability and trafficking. Thus far, there has not been any investigation into the role of flotillin-1 palmitoylation in the context of metastasis in vivo. To address the role of flotillin-1 palmitoylation in metastasis, MDA-MB-231 cells expressing palmitoylation defective flotillin-1 constructs were used as models. Compared to flotillin-1 WT expressing tumors, flotillin-1 palmitoylation defective displayed abrogated tumor progression and lung metastasis in vivo in both spontaneous and experimental models. Further mechanistic investigation led to the identification of zDHHC5 as the main palmitoyl acyltransferase responsible for palmitoylating endogenous flotillin-1. Modulation of flotillin-1 palmitoylation status through mutagenesis, zDHHC5 silencing, and 2-bromopalmitate inhibition all resulted in the proteasomal degradation of flotillin-1 protein. To assess if flotillin-1 palmitoylation can be inhibited for potential clinical relevance, we designed a competitive peptide fused to a cell penetrating peptide sequence, which displayed efficacy in blocking flotillin-1 palmitoylation in vitro without altering palmitoylation of other zDHHC5 substrates, highlighting its specificity. Additionally, TNBC xenograft tumor models expressing a doxycycline inducible flotillin-1 palmitoylation inhibiting peptide displayed attenuated tumor growth and lung metastasis. Collectively, these results reveal a novel palmitoylation dependent mechanism which is essential for the stability of flotillin-1 protein. More specifically, disruption of flotillin-1 palmitoylation through mutagenesis or competitive peptide promoted flotillin-1 protein degradation, subsequently impeding its tumor promoting and metastasis-inducing effects in TNBC tumor models.

Introduction

Triple negative breast cancer (TNBC) is an aggressive subtype of breast cancer characterized by its high propensity to metastasize (1). Though there has been success in targeted therapies for other subtypes of breast cancer, TNBC therapies are mainly limited to highly cytotoxic chemotherapeutic approaches (1). Thus, there is a great need to uncover novel therapeutic targets in TNBC as well as mechanisms of metastasis, of which results in over 90% of TNBC associated mortality (1).

Flotillins are a class of proteins enriched in lipid rafts within plasma membranes (2, 3, 4). Flotilln-1 and 2 often hetero-oligomerize with one another and offer stable signaling platforms for receptors in addition to promoting their intracellular trafficking, stability, and signaling (5). Recently, it has been found that flotillins contribute to a protein trafficking process termed upregulated flotillin-induced trafficking (UFIT), which involves aberrant plasma membrane invaginations that contribute to exacerbated receptor signaling from non-degradative late endosomal compartments (6, 7).

Flotillin protein expression is often lower in normal cells, however it is upregulated in many solid tumors (8). Moreover, its expression is associated with invasion and metastasis (8). Various findings have implicated flotillin-1 as a biomarker for lymph node metastasis including one study investigating

flotillin-1 expression in lung adenocarcinoma through the utilization of unbiased membrane proteomics (9, 10). Flotillin upregulation in numerous cancers has been associated with transforming growth factor beta (TGF-β) (11), Axl (6) , and Insulin-like growth factor-1 receptor (IGF-1R) signaling (2, 12) , all of which contribute to tumor progression and metastasis.

Flotillin-1 is modified by SUMOylation, phosphorylation, and S-palmitoylation (2, 13, 14). S-palmitoylation is the process of transferring palmitoyl-CoA to proteins which is catalyzed through a class of zDHHC palmitoyl acyltransferase enzymes (15). Palmitoylation through zDHHC enzymes modulates protein stability, trafficking, and processing (16, 17). Given the strong evidence that flotillin-1 expression contributes to cancer metastasis, we questioned if its palmitoylation could be a contributing factor in its tumor promoting and metastasis-inducing capabilities (9, 10, 11).

By constructing MDA-MB-231 TNBC cell lines to stably express a palmitoylation-defective form of flotillin-1, we demonstrate that fotillin-1 palmitoylation is essential for its stability as well as its capacity to promote tumor growth and lung metastasis *in vivo*. Further investigation led to the discovery of zDHHC5 as the main palmitoyl acyltransferase responsible for palmitoylating endogenous flotillin-1, which was found to contribute to its stability by preventing its poly-ubiquitylation. Finally, we provide proof-of-concept data through the utilization of a palmitoylation inhibiting competitive peptide, demonstrating flotillin-1 palmitoylation as an actionable therapeutic target in TNBC.

Materials and Methods

Data and code availability

Bulk RNA-seq has been data has been deposited at GEO under the accession number **GSE236971,** which will be accessible upon the publication of this study. All the code used in the analysis of the RNA-seq data was already established from various R studio packages listed in RNA-seq data analysis. Any additional information or data will be made available upon request.

Cell Culture

MDA-MB-231, SUM-159, and HEK 293T were purchased from ATCC and cultured in DMEM + 10% FBS + 1x Anti-Anti. MCF-7 were purchased from ATCC cultured in DMEM + 10% FBS + 10ug/ml insulin + 1x Anti-Anti. MCF-10A were purchased from ATCC and cultured in DMEM + 10% FBS + .5 mg/ml hydrocortisone + 20 ng/ml EGF+ 10ug/ml insulin+ 100 ng/ml cholera Toxin + 1x Anti-Anti. All cells were routinely tested for mycoplasma by PCR test. Cells were grown in an incubator at 37° C + 5% CO_2 with maintained humidity. Upon initial acquisition, cell lines were passaged 2-4 times prior to generating large amounts of aliquots for freezing and storage in liquid nitrogen. Upon thawing, cells were not passaged more than 20 times.

Animal Experiments

All experiments were conducted within AAALAC guidelines and were approved by the University of Texas Institutional Animal Care and Use Committee (Protocol No. AUP-2022-00082). Six-to-eight week old FOX Chase SCID Beige mice (Charles River laboratories, strain code: 250) were injected bilaterally with $1x10^5$ WT or C34A flotillin-1 expressing MDA-MB-231 shFlotillin-1 3` UTR cells also labelled with GFP and dTomato reporters, respectively. The cells were suspended in a 1:1 ratio of PBS to Matrigel (50ul PBS: 50ul Matrigel) and injected orthotopically into the 4^{th} mammary fat pad. Tumor diameter and mouse weight was monitored bi-weekly to ensure there were no significant changes in weight or that the tumor diameter did not exceed 1.5 cm. After 8-weeks of growth, animals were euthanized, and tissues were processed for imaging as described in the immunofluorescence section.

For experimental lung metastasis experiments, $.5x10^6$ MDA-MB-231 shFlotillin-1 3` UTR cells expressing flotillin-1 C34A or WT constructs along with a luciferase reporter lentiviral vector were injected into the lateral tail vein of six-to-eight week old SCID Beige (Charles River laboratories) . Mice were injected with intraperitoneally 150 ul of D-luciferin in sterile PBS (30mg/ml) and anesthetized with 3% isoflurane prior to BLI images using the IVIS. Images were taken at day 0, 7, 14, 21, and 28 in mice. Lungs were then removed and placed in 12-well dishes containing PBS for *Ex Vivo* lung imaging on day 28. Images were analyzed using IVIS living imaging software.

For doxycycline-induced flotillin-1 peptide experiments, $1x10^6$ MDA-MB-231 or SUM-159 luciferase-mCherry along with either F1C or F1A (control) peptide expressing cells were injected into the #4 mammary fat pad of six-to-eight week old SCID Beige mice at a 1:1 ratio of PBS: Matrigel. Upon palpable tumor establishment, mice were switched to a diet consisting of 200 mg/kg of doxycycline. Luciferase images were obtained weekly by IP injection of 150 ul of PBS solution containing 30mg/ml of D-luciferin.

Fluorescence Activated Cell Sorting

Primary tumors were minced with a scalpel and placed in DMEM containing 2mg/mL of collagenase A + 100 units of DNase I. Tumors were digested at 37° C for three hours and then passed through a 70 µM nylon cell strainer to create a single cell suspension. To isolate lungs from mice for mCherry+ cancer cell quantification, lungs were minced with a razor blade and placed in a 6-well dish containing 5mL of digestion medium consisting of 2mg/mL collagenase A + .25mg/ml of hyaluronidase+100 units of DNAse I in DMEM + 10% FBS and incubated at 37 º C for 1 hour in a shaking incubator. Cell suspension was then filtered through a 40-uM cell strainer, spun down, and resuspended in 1ml of ACK red blood cell lysis buffer for 5 minutes at room temperature to lyse red blood cells.

Both cell suspensions from primary tumors or lungs were then spun down and re-suspended in PBS + 2% FBS. Non-fluorescent parental MDA-MB-231 cells as well as digested lungs from non-tumor bearing mice were also suspended in the same buffer and used as non-fluorescent controls. Cell sorting was performed using a BD FACS Aria Fusion at the Center for Biomedical Research Support Microscopy and Imaging

Facility at UT Austin (RRID# SCR_021756). Gating strategies can be found in the supplemental information.

Peptide Treatments

CPP and CPP-F1 peptides were synthesized by ABclonal and delivered as a lyophilized powder. The peptides were re-suspended in sterile nuclease-free water to make a concentrated stock of 1200 uM and 500 uM, respectively. The peptides were then aliquoted and stored at -80 protected from light until use. Peptides were added to culture medium at desired concentrations for 24 hours for in vitro treatments.

For *in vivo* peptide treatments, CPP-F1 peptide was diluted to a concentration of 1ug/ul in sterile H20 and intraperitoneally I.P. injected into tumor bearing SCID beige mice at a concentration of 150ug/mouse (150ul). Mice received I.P. injections of 150ul of water for the water only controls.

Statistical Analysis

Data are represented as mean SD or SEM. *P* values in the study were calculated by performing two-sided Students t-test. Differences between the two groups were significant if the *P* value was below 0.05. Pearson's Correlation coefficient was also performed using NIH Image J software to detect colocalization. Due to unequal sample sizes of the mice in figure 3, a Mann-Whitney *U*-test was performed instead of a two-sided students t-test.

For complete descriptions of materials and methods please refer to the supplementary materials and data file.

Results

1. Modulation of flotillin-1 palmitoylation alters its stability and membrane localization.

Flotillin-1 is highly expressed in triple negative breast cancer (TNBC) and its expression is associated with metastasis (6, 18). We further confirmed its high expression in TNBC by probing for flotillin-1 protein in a panel of TNBC cell lines, of which revealed high flotillin-1 expression compared to that of luminal (ER+), MCF-7, and non-cancerous (NC) MCF-10A cells (Fig. 1a). Using MCF-10A cells to represent non-cancerous cell populations, we depleted flotillin-1 protein even further through RNAi and did not observe any apoptosis or altered cell viability compared to control, as measured by cleaved-PARP and MTT assay, respectively (Supplementary Fig. 1 a,b). With the preponderance of studies demonstrating the role of flotillin-1 protein expression in cancer progression and metastasis (4, 8, 9), we sought to develop a model to study the effects of its palmitoylation in the context of TNBC metastasis. To this end, we constructed flotillin-1 palmitoylation defective mutants by mutating its palmitoylated cysteine 34 reside to an alanine, a mutation previously used to study its cellular localization (2). Both the floillin-1 wild type (WT) and palmitoylation defective (C34A) constructs were cloned into an eGFP vector to generate GFP fusion proteins (Fig. 1b). We further confirmed the palmitoylation defect through click chemistry and GFP western blotting in HEK 293T cells (Fig.1c). MDA-MB-231 TNBC cells were chosen as the host cell line for

the constructs given their high expression of flotillin-1 protein and their ubiquitous use in xenograft models of TNBC metastasis. To avoid any complications with the high level of endogenous flotillin-1 expression, we transduced these MDA-MB-231 cells with a 3' untranslated region (UTR) targeted shRNA against endogenous flotillin-1 (shF1), which allows for the re-expression of flotillin-1 cDNA (Supplementary Fig.1, d). Upon re-expression of C34A flotillin-1 in shF1 cells, we observed a surprising reduction in ectopically expressed flotillin-1 C34A protein compared to WT (Fig. 1d). To ensure these results were not due to transcription discrepancies between the two constructs, we performed RT-PCR for flotillin-1 mRNA between flotillin-1 WT and C34A expressing cells and found no difference in mRNA levels, suggesting the loss of protein in the C34A flotillin-1 was post-transcriptional (Fig. 1e). For further analysis, we generated stably expressing WT and C34A flotillin-1 cells by transducing shF1 MDA-MB-231 cells with flotillin-1 WT or C34A lentiviral constructs, which still harbored the C34A palmitoylation defect after stable integration and did not display any changes in cell viability (Supplementary Fig. 1a,c). Numerous studies have demonstrated flotillin-1 and 2 protein expression to be dependent on one another (18, 19, 20, 21, 22). Commensurate with these findings, we observed reduction in flotillin-2 protein upon both flotillin-1 depletion and re-expression of flotillin-1 C34A protein (Supplementary Fig 1 d,e). Though we can still visualize and detect flotillin-1 directly through specific antibodies, the role of the additional loss of flotillin-2 on any phenotypic effects observed cannot be ruled out. Palmitoylation can protect proteins from degradation by altering their stability (23, 24). We next asked if the observed protein loss in the flotillin-1 palmitoylation defective construct was due to a decrease in its protein stability. To assess the stability of flotillin-1, we performed a cycloheximide (CHX) chase assay, which revealed an accelerated degradation of the flotillin-1 C34A protein compared to WT (Fig 1f). Palmitoylation of proteins can prevent both lysosomal and proteasomal degradation (23, 25), which motivated us to explore the method in which the flotillin-1 C34A protein degradation was occurring. To discern how flotillin-1 C34A protein was being degraded, we performed rescue experiments with empirically validated (Supplementary Fig. 2 c,d) concentrations of proteasomal (MG-132) or lysosomal (Chloroquine, CQ) inhibitors after depleting flotillin-1 C34A protein with CHX. Flotillin-1 C34A protein levels were significantly restored upon MG-132 treatment, while chloroquine failed to restore flotillin-1 C34A protein (Fig. 1g). The flotillin-1 WT expressing cells were also included as a control and did not display any significant protein alterations with the same conditions (Fig. 1g). The method used for detecting protein palmitoylation with click chemistry requires the enrichment of palmitoylated proteins with streptavidin. To ensure the loss of palmitoylation observed with the flotillin-1 C34A mutation was not due to a decrease in available protein for streptavidin enrichment, we repeated the click chemistry labeling and enrichment method with MG-132 treatment, which restored flotillin-1 C34A protein levels without affecting its palmitoylation status, further confirming its palmitoylation defect (Fig. 1h). To ensure these observations were not specific to ectopic expression of flotillin-1, we treated MDA-MB-231 and SUM 159 TNBC cell lines with a global palmitoylation inhibitor (2-bromopalmitate, 2-BP) with or without MG-132. 2-BP treatment significantly decreased endogenous flotillin-1 protein expression in both cell lines, which was effectively restored upon treatment with MG-132 (Supplementary Fig. 2b). Flotillin-1 palmitoylation was initially studied based on its involvement in its plasma membrane trafficking (2). To assess if the palmitoylation defect was also altering flotillin-1 plasma membrane localization, we performed immunofluorescence in MDA-MB-231

cells expressing a wild type flotillin-1 fused to eGFP and flotillin-1-C34A fused to dTomato. Counter staining with the plasma membrane marker, Na+/K+ ATPase, revealed in a high colocalization with the wild type flotillin-1, compared to the palmitoylation defective flotillin-1 (C34A), even when the protein expression was restored with MG-132 treatment (Fig. 1h). The observed altered flotillin-1-C34A plasma membrane localization prompted us to determine if the flotillin-1 palmitoylation defect was modifying its ability to exit out of the endoplasmic reticulum (ER) or Golgi, given the role of palmitoylation and proper protein processing (2, 26, 27). Counterstaining with ER (Calreticulin) and Golgi (GM-130) specific antibodies revealed no ER or Golgi retention of flotillin-1 C34A (Supplementary Fig. 2e). Collectively, the current results demonstrate an attenuated protein stability and plasma membrane localization upon flotillin-1 palmitoylation modulation.

2. zDHHC5 contributes to the stability of endogenous flotillin-1 by preventing its proteasomal degradation.

Palmitoyl acyltransferases or zDHHCs are the enzymes responsible for transferring palmitoyl-CoA to target proteins (25, 28, 29). To identify the zDHHC enzyme responsible for palmitoylating endogenous flotillin-1, we performed a mini shRNA screen against the three highest expressing zDHHC enzymes in breast cancer based on data from the human protein atlas (Fig. 2a). After confirming the specificity and knockdown efficiency of the shRNAs by RT-PCR or western blotting, we analyzed flotillin-1 palmitoylation levels in the different stable zDHHC knockdown cell lines (Supplementary Fig. 3 a,b , Fig. 2b). zDHHC 5 knockdown substantially reduced flotillin-1 palmitoylation status compared control, zDHHC 17 and 21 shRNA expressing cells. These findings were also confirmed in MDA-MB-231 and SUM-159 TNBC cell lines without any observed cell viability alterations upon zDHHC5 silencing (Fig. 2d, Supplementary Fig. 3c, e). The palmitoylation sate of two additional zDHHC5 substrates (EZH2 and flotillin-2) were also found to be substantially decreased in the zDHHC5 silenced cells compared to the other conditions (Supplementary Fig. 3d) (28, 30). We further observed a high colocalization between zDHHC5 and flotillin-1 by immunofluorescence (Fig. 2c). The zDHHC5 knockdown cells were subsequently used as a model to study the effect of endogenous flotillin-1 palmitoylation. As before, we performed CHX stability assays and found a decrease in flotillin-1 protein stability in the zDHHC5 knockdown compared to control cells (Fig. 2e). To further confirm that this degradation was through the proteosome, we performed rescue experiments with MG-132 treatment, which effectively restored flotillin-1 protein levels in the presence of CHX compared to vehicle control (Fig. 2f). Given that a 26S proteosome inhibitor (MG-132) was restoring protein expression in the zDHHC5 silenced cells, we questioned if blocking palmitoylation was increasing flotillin-1 poly-ubiquitination. To analyze the poly-ubiquitination state of flotillin-1, we utilized tandem ubiquitin binding entities (TUBE), a poly-ubiquitin resin conjugated to biotin, which allows for streptavidin enrichment and western blotting of the pulldown fraction which contains the poly-ubiquitylated proteins. Cell lysates from control or zDHHC5 knockdown cells, were incubated with or without the biotin conjugated TUBE and isolated by streptavidin enrichment (Fig. 2g). Western blotting of the enriched lysates revealed that zDHHC5 knockdown significantly increased the poly-ubiquitination of flotillin-1 (Fig. 2h), suggesting that zDHHC5 mediated flotillin-1 palmitoylation effects its stability by preventing its ubiquitin mediated proteasomal degradation.

3. Flotillin-1 palmitoylation defective TNBC cells display attenuated tumor growth and lung metastasis.

We initially observed *in vitro* that the flotillin-1 C34A expressing cells displayed decreased invasive capacities compared to flotillin-1 WT using collagen-I coated trans well membranes (Supplementary Fig. 4a) To test if these *in vitro* findings would translate into metastasis *in vivo*, we utilized our shF1 MDA-MB-231 cells stably re-expressed with flotillin-1 WT and C34A. Flotillin-1 WT and C34A cells were then counter labelled with lentiviral GFP and dTomato reporters, respectively, to track metastasis.

Flotillin-1-WT-GFP and flotillin-1-C34A-dTomato expressing MDA-MB-231 cells were subsequently implanted bilaterally into the left and right #4 mammary fat pad of SCID beige mice (Fig. 3 a,b). After 8 weeks of tumor growth, we analyzed both primary tumor size and lungs for metastasis (n=5 mice). At the end of the 8-week growth period, there was a significant reduction in primary tumor weight in the C34A vs WT tumors (Fig. 3c). We also assessed tumor proliferation and apoptosis by IHC staining for Ki67 and cleaved-caspase 3, respectively. IHC staining of the primary tumor sections revealed substantially less Ki67 staining in the C34A compared to WT (Fig. 3d). From the 5 mice, two WT and C34A flotillin-1 mice were selected for FACS sorting to isolate GFP+ and dTomato+ cells from these tumors for bulk RNA sequencing (Fig. 3e, Supplementary Fig. 4b). Differential expression analysis resulted in 1,118 upregulated and 570 downregulated transcripts between C34A vs WT flotillin-1 expressing tumors when filtered based on an absolute log2fold change of ±1 (Fig. 3e). Gene ontology analysis revealed a down-regulation of transcripts associated with cell motility, receptor signaling, and inflammatory responses while there was an up-regulation of transcripts involved in ion transport and membrane depolarization in C34A expressing cells vs WT (Fig. 3f., Supplementary Fig. 4. d,e). Gene set enrichment analysis also confirmed a negative enrichment in gene sets involved in cell taxis as well as NF-kb and MAPK signaling in the C34A flotillin-1 expressing tumors vs WT, in line with the gene ontology analysis (Supplementary Fig. 4c). We subsequently identified five transcripts from our differential expression analysis (absolute log2fold change ± 1.5) that were also present in a 14 mRNA TNBC lung metastasis signature (31), including CXCL2, SELL, CD36, ICAM1, and G0S2. Collectively, these results demonstrate the ability of flotillin-1 palmitoylation inhibition to alter the migratory and metastatic cell phenotype at the transcript level (Fig. 3h). To assess if the transcriptional metastatic phenotype observed would translate to a functional phenotype, lungs from WT and C34A flotillin-1 tumor bearing mice (n=5) were analyzed for GFP+ and dTomato+ lung metastases. GFP and dTomato lung section immunostaining revealed multiple cases of multi-cellular GFP+ micro metastatic lung lesions with no observed dTomato+ (Fig 3 i,j). The absence of dTomato+ lung metastatic cells could be due to the drastically smaller primary tumor size and consequently less available cells to seed into circulation rather than an attenuated metastatic capability.

To ensure that the observed loss in lung metastasis from the C34A flotillin-1 expressing tumors was not merely due to a smaller number of cells initializing the metastatic cascade, we utilized an experimental lung metastasis model which removes the factor of primary tumor size and focuses on later stages of metastasis after cells have begun hematogenous dissemination. In this model, an equal number ($5x10^5$) of flotillin-1 WT and C34A luciferase expressing MDA-MB-231 cells were intravenously injected into the

lateral tail vein of SCID beige mice (WT n=3, C34A n=4). Photon flux from the bioluminescence (BLI) imaging revealed a significant reduction in lung metastasis from the flotillin-1 C34A cells compared to WT (Fig. 3 k, l). Lung metastasis was further confirmed by performing H&E staining of lung sections (Fig. 3k). The current results demonstrate flotillin-1 palmitoylation to be an essential biological process for tumor progression and successful establishment of lung metastasis in a TNBC xenograft model.

4. Targeting flotillin-1 palmitoylation with a competitive peptide attenuates tumor growth and lung metastasis.

We have demonstrated that altering the palmitoylation status of flotillin-1 results in its degradation and attenuated tumor progression *in vivo.* In order to assess the ability to target this process for potential therapeutic benefit, we designed a competitive targeting peptide containing the palmitoylation sequence of flotillin-1, a strategy previously employed to block the palmitoylation of other proteins in preclinical models of solid tumors (29, 32). To study the effect of a palmitoylation blocking peptide *in vitro*, the coding sequence corresponding to flotillin-1 amino acid sequence (23-42) was cloned into a eGFP lentiviral vector. We subsequently transduced MDA-MB-231 cells with either an empty eGFP vector (GFP-EV) for a control or the flotillin-1 peptide sequence (23-42) fused to GFP (GFP-F1). For the peptide to successfully block endogenous flotillin-1 palmitoylation, it must first become palmitoylated, presumably through zDHHC5, to saturate the palmitate that is destined for flotillin-1 modification. We subsequently performed click chemistry labeling in MDA-MB-231 cells alone, expressing an empty GFP vector (GFP-EV), or expressing the flotillin-1 peptide fused to GFP (GFP-F1) to assess the ability of the flotillin-1 peptide to become palmitoylated. Click labeling revealed high levels of palmitoylation in the GFP-F1 peptide compared to that of GFP alone (Fig. 4a). To determine if the GFP-F1 peptide palmitoylation was through zDHHC5, we expressed the GFP-F1 peptide in shControl or shzDHHC5 cells followed by click chemistry labeling. GFP pulldown of the labelled proteins revealed a drastic reduction in GFP-F1 palmitoylation in the zDHHC5 depleted cells compared to control (Fig. 4b). Importantly, we found the zDHHC5 induced palmitoylation of the GFP-F1 peptide to substantially reduce the palmitoylation of endogenous flotillin-1 ostensibly by acting as a zDHHC5 palmitoylation decoy (Fig. 4d, Supplementary Fig. 6a). To study the ability to block flotillin-1 palmitoylation in a more therapeutically relevant manor, we fused the flotillin-1 palmitoylation targeting peptide sequence to a CPPtat , a well-known peptide sequence that encourages cellular uptake of therapeutics into cells (33) (Fig. 4e). *In vitro* treatment with the flotillin-1 peptide (CPP-F1) successfully inhibited flotillin-1 palmitoylation in MDA-MB-231 cells, without altering the palmitoylation state of two other zDHHC5 substrates, EZH2 and flotillin-2 (Fig. 4f). We further observed that this peptide decreased total flotillin-1 protein expression in both MDA-MB-231 and SUM-159 cells, providing *in vitro* evidence of successful flotillin-1 protein targeting through the delivery of a palmitoylation inhibiting peptide (Fig. 4g, Supplementary Fig. 6b). Knowing that the flotillin-1 peptide sequence successfully targets endogenous flotillin-1 protein palmitoylation, we questioned if this would provide any benefit in TNBC tumor progression *in vivo.* For this analysis, we utilized the delivery of the peptide through a lentiviral vector rather than fused to a CPPtat sequence to ensure that the peptide would be successfully delivered into the cells. The doxycycline inducible system was further utilized to provide temporal control of the flotillin-1 peptide expression. To generate these inducible flotillin-1

palmitoylation targeting constructs, we subcloned the flotillin-1 coding sequence corresponding to its amino acids (23-42) into tetracycline inducible lentiviral vector containing an eGFP to generate a GFP-flotillin-1 targeting peptide fusion, which was termed F1C (Fig 4g). We also subcloned a mutated (C34A) flotillin-1 peptide sequence into the same backbone vector as a control, further referred to as F1A (Fig. 4g). There was no observed GFP-peptide expression in the absence of doxycycline, suggesting no promoter leakiness (Supplementary Fig. 5a). Subsequent *in vitro* analysis revealed a reduction in flotillin-1 protein and palmitoylation status upon doxycycline addition in the F1C vs F1A cells (Supplementary Fig. 5b-c.) To assess the ability to target flotillin-1 protein *in vivo* through the delivery of a competitive peptide, MDA-MB-231 TNBC cells engineered to express either F1C or F1A constructs as well as a bicistronic dual mCherry-luciferase reporter were implanted into the #4 mammary fat pads of SCID beige mice to induce tumors. Upon palpable tumor detection, mice were switched to a diet containing 200 mg/kg of doxycycline to activate the expression of the flotillin-1 targeted (F1C) or control (F1A) peptides in the xenografted tumors. BLI detection of the primary tumors showed no change in tumor growth prior to the addition of doxycycline (Supplementary Fig. 5d), however, after 8-weeks of growth, there was a significant reduction in primary tumor weight (n=3) in the F1C vs F1A mice (Fig. 4 h,i, Supplementary Fig. 5d). Primary tumors were subsequently analyzed to detect levels of flotillin-1 palmitoylation, by acyl-biotin exchange (experimental details in materials and methods), which revealed substantial flotillin-1 palmitoylation inhibition in F1C tumors compared to F1A. It was further confirmed that F1C targeting peptide significantly decreased flotillin-1 total protein expression in primary tumors (n=3) compared to that of F1A control (Fig. 4l). To assess if targeting flotillin-1 palmitoylation and protein in the primary tumor would result in decreased metastasis, we performed *ex vivo* BLI detection in the lungs of tumor bearing mice. Unfortunately, we found that only two out of three lungs from the F1A mice contained metastasis large enough to be detected by BLI (Fig. 4h). As an alternative, we utilized the mCherry reporter that the cells also harbored to assess lung metastasis by FACS (Fig. 4j). When single cell suspensions from the lungs of tumor bearing mice were subjected to FACS analysis for mCherry expression, there was a significant reduction in percentage of mCherry+ cancer cells in the lungs of F1C vs F1A mice (n=3) (Fig 4j). We repeated this experiment using SUM-159 xenografted tumors, which also did not display altered tumor growth prior to doxycycline administration (Supplementary Fig. 6c). Surprisingly, there was an observed tumor regression post-doxycycline administration in both F1A and F1C mice that lead to an early termination point at week 7 instead of week 8. Regardless, we observed a pronounced decrease in tumor BLI in F1C vs F1A tumors (Supplementary Fig. 6 c,d). Shockingly, we did not observe any tumors (0 out of 3 mice) in the F1C mice compared to F1A, which contained established tumors 2 out of 3 mice (Supplementary Fig. 6 c,d,f). Given the ability of the expressed peptide from a lentiviral vector to target flotillin-1 protein *in vivo,* we questioned if it could be delivered in the same format we utilized *in vitro.* To this end, we dissolved the flotillin-1 targeting CPP-F1 peptide in water and administered it by I.P. injection to tumor bearing mice along with water only injections as a control. 24 hours post injection, tumors were analyzed for total flotillin-1 protein. Treatment with 150ug of CPP-F1 peptide substantially reduced flotillin-1 protein in tumors compared to water only controls (n=2) (Fig. 4m). Collectively, these results demonstrate the ability to target flotillin-1 protein in *vivo* through delivery of a competitive peptide and provide proof-of-concept data demonstrating flotillin-1 targeted peptide delivery

as an effective strategy to promote its degradation and subsequently impede tumor growth and metastasis in xenograft models of TNBC.

Discussion

The current study demonstrates an essential role of palmitoylation in the stability of flotillin-1 in TNBC. Specifically, inhibiting palmitoylation of flotillin-1 through mutagenesis as well as silencing the palmitoyl acyltransferase responsible for its palmitoylation contributes to its proteasomal degradation. Further analysis revealed the potential to target flotillin-1 palmitoylation through a competitive peptide, which promoted its degradation and led to a significant decrease in tumor growth and lung metastasis in TNBC xenografted tumor models.

To our knowledge, we are the first study to demonstrate flotillin-1 palmitoylation in mediating its protein stability, specifically through minimizing its poly-ubiquitination and proteasomal degradation. Palmitoylation has been demonstrated to protect proteins from the ubiquitin-proteasomal system, which is in accordance with our current findings (23, 26). Further, we identified the zDHHC5 as the primary palmitoyl acyltransferase enzyme responsible for palmitoylating flotillin-1 in TNBC cell lines. zDHHC5 is highly expressed in multiple cancers including breast, however, our results contradict other findings which indicate zDHHC19 as the primary enzyme responsible for palmitoylating flotillin-1 (34). An explanation for this discrepancy could be due to differing tissue specific expression of zDHHC19, which is not highly expressed in breast cancer tissues (34). Thus, our reported observations could be a mechanism that is dependent upon zDHHC5 flotillin-1 palmitoylation and not palmitoylation from other zDHHC enzymes which warrants further investigation in other cancers that highly express zDHHC5 such as glioma (30) and pancreatic (35).

Targeting flotillin-1 palmitoylation through competitive peptide demonstrated evidence of promoting its degradation *in vitro.* To this end, we engineered cancer cell lines to express the peptide from a doxycycline inducible lentiviral construct, which effectively attenuated lung metastasis and blunted tumor growth in cell line xenografted TNBC tumors. Palmitoylation targeting peptides have been utilized previously, but have variations in their stability *in vivo*, hence our use of the lentiviral peptide delivery *(29, 32).* Additionally, this proof-of-concept method provided a tool to study the effects of endogenous flotillin-1 palmitoylation on the biology of TNBC tumor progression and metastasis, which will potentially offer insight into alternative models to study the effects of protein palmitoylation *in vivo.* Currently, most studies accomplish *in vivo* investigation of protein palmitoylation through mutagenesis, global palmitoylation inhibition, or modulating zDHHC enzyme expression. The flotillin-1 blocking peptide did not alter the palmitoylation of other zDHHC5 substrates, thus this method of palmitoylation modulation could limit off target effects and increase the interpretability of phenotypic results *in vivo.*

The lack of tumor growth in the SUM-159 xenograft model hindered the ability to analyze primary tumors, given there were no observed tumors in the F1C targeted group. This regression in growth could be due to the SUM-159 sensitivity to larger doses of doxycycline (36) that were not present during *in vitro* culture,

but could have been through administration by feed to activate the peptides *in vivo*. Unfortunately, we did not collect an adequate amount of blood from the mice to measure concentrations of doxycycline in individual mice and did not perform a pilot study, given our positive results from the MDA-MB-231 xenograft. Though we are comfortable with the fact that when mice were given the same weight of doxycycline chow, there was a pronounced difference in tumor growth and complete lack of established tumors at the end point in the targeted peptide (F1C) compared to control (F1A). Additionally, our *in vitro* observations demonstrate that the SUM-159 peptide engineered cells displayed substantial reduction in flotillin-1 protein and palmitoylation upon expression of the targeting (F1C) vs control peptide (F1A).

Collectively, we have highlighted a novel mechanism of flotillin-1 protein stability mediated through zDHHC5 palmitoylation as well as explored methods in targeted flotillin-1 palmitoylation inhibition through the delivery of a competitive peptide. Strategies to understand and target proteins contributing to TNBC metastasis will be vital for improving future treatments and patient outcomes.

Declarations

Acknowledgements

We would like to thank Dr. Brittany Harlow for offering her support during data collection as well as the UT Austin flow cytometry core for their support with the FACS experimentation.

References

1. Desantis CE, Ma J, Gaudet MM, Newman LA, Miller KD, Goding Sauer A, et al. Breast cancer statistics, 2019. CA: A Cancer Journal for Clinicians. 2019;69(6):438-51.
2. Jang D, Kwon H, Jeong K, Lee J, Pak Y. Essential role of flotillin-1 palmitoylation in the intracellular localization and signaling function of IGF-1 receptor. J Cell Sci. 2015;128(11):2179-90.
3. Amaddii M, Meister M, Banning A, Tomasovic A, Mooz J, Rajalingam K, et al. Flotillin-1/reggie-2 protein plays dual role in activation of receptor-tyrosine kinase/mitogen-activated protein kinase signaling. Journal of Biological Chemistry. 2012;287(10):7265-78.
4. Koh M, Yong HY, Kim ES, Son H, Jeon YR, Hwang JS, et al. A novel role for flotillin-1 in H-R as-regulated breast cancer aggressiveness. International journal of cancer. 2016;138(5):1232-45.
5. Morrow IC, Rea S, Martin S, Prior IA, Prohaska R, Hancock JF, et al. Flotillin-1/Reggie-2 Traffics to Surface Raft Domains via a Novel Golgi-independent Pathway: IDENTIFICATION OF A NOVEL MEMBRANE TARGETING DOMAIN AND A ROLE FOR PALMITOYLATION. 2002;277(50):48834-41.
6. Genest M, Comunale F, Rios-Morris E, Planchon D, Govindin P, Vacher S, et al. Flotillin-upregulation acts as an epithelial-mesenchymal transition driver by promoting sphingosine kinase 2-dependent AXL stabilization. bioRxiv. 2020:2020.05. 12.090571.
7. Planchon D, Morris ER, Genest M, Comunale F, Vacher S, Bièche I, et al. MT1-MMP targeting to endolysosomes is mediated by upregulation of flotillins. Journal of cell science. 2018;131(17).

8. Ou Y, Liu F, Chen F, Zhu Z. Prognostic value of Flotillin-1 expression in patients with solid tumors. Oncotarget. 2017.
9. Li Z, Yang Y, Gao Y, Wu X, Yang X, Zhu Y, et al. Elevated expression of flotillin-1 is associated with lymph node metastasis and poor prognosis in early-stage cervical cancer. American journal of cancer research. 2016;6(1):38.
10. Zhang P-F, Zeng G-Q, Hu R, Li C, Yi H, Li M-Y, et al. Identification of flotillin-1 as a novel biomarker for lymph node metastasis and prognosis of lung adenocarcinoma by quantitative plasma membrane proteome analysis. Journal of proteomics. 2012;77:202-14.
11. Cao S, Cui Y, Xiao H, Mai M, Wang C, Xie S, et al. Upregulation of flotillin-1 promotes invasion and metastasis by activating TGF-β signaling in nasopharyngeal carcinoma. Oncotarget. 2016;7(4):4252.
12. Dam DHM, Jelsma SA, Yu JM, Liu H, Kong B, Paller AS. Flotillin and AP2A1/2 Promote IGF-1 Receptor Association with Clathrin and Internalization in Primary Human Keratinocytes. Journal of Investigative Dermatology. 2020.
13. Jang D, Kwon H, Choi M, Lee J, Pak Y. Sumoylation of Flotillin-1 promotes EMT in metastatic prostate cancer by suppressing Snail degradation. Oncogene. 2019.
14. Riento K, Frick M, Schafer I, Nichols BJ. Endocytosis of flotillin-1 and flotillin-2 is regulated by Fyn kinase. Journal of cell science. 2009;122(7):912-8.
15. Wang Y, Lu H, Fang C, Xu J. Palmitoylation as a Signal for Delivery. Springer Singapore; 2020. p. 399-424.
16. Coleman DT, Gray AL, Kridel SJ, Cardelli JA. Palmitoylation regulates the intracellular trafficking and stability of c-Met. Oncotarget. 2016;7(22):32664.
17. Ernst AM, Syed SA, Zaki O, Bottanelli F, Zheng H, Hacke M, et al. S-Palmitoylation Sorts Membrane Cargo for Anterograde Transport in the Golgi. Developmental Cell. 2018;47(4):479-93.e7.
18. Berger T, Ueda T, Arpaia E, Chio I, Shirdel E, Jurisica I, et al. Flotillin-2 deficiency leads to reduced lung metastases in a mouse breast cancer model. Oncogene. 2013;32(41):4989-94.
19. Ludwig A, Otto GP, Riento K, Hams E, Fallon PG, Nichols BJ. Flotillin microdomains interact with the cortical cytoskeleton to control uropod formation and neutrophil recruitment. Journal of Cell Biology. 2010;191(4):771-81.
20. Frick M, Bright NA, Riento K, Bray A, Merrified C, Nichols BJ. Coassembly of flotillins induces formation of membrane microdomains, membrane curvature, and vesicle budding. Curr Biol. 2007;17(13):1151-6.
21. Langhorst MF, Solis GP, Hannbeck S, Plattner H, Stuermer CA. Linking membrane microdomains to the cytoskeleton: regulation of the lateral mobility of reggie-1/flotillin-2 by interaction with actin. Febs Letters. 2007;581(24):4697-703.
22. Babuke T, Ruonala M, Meister M, Amaddii M, Genzler C, Esposito A, et al. Hetero-oligomerization of reggie-1/flotillin-2 and reggie-2/flotillin-1 is required for their endocytosis. Cellular signalling. 2009;21(8):1287-97.

23. Kong C, Lange JJ, Samovski D, Su X, Liu J, Sundaresan S, et al. Ubiquitination and degradation of the hominoid-specific oncoprotein TBC1D3 is regulated by protein palmitoylation. Biochemical and biophysical research communications. 2013;434(2):388-93.
24. Yang Y, Hsu J-M, Sun L, Chan L-C, Li C-W, Hsu JL, et al. Palmitoylation stabilizes PD-L1 to promote breast tumor growth. Cell research. 2019;29(1):83-6.
25. Yao H, Lan J, Li C, Shi H, Brosseau J-P, Wang H, et al. Inhibiting PD-L1 palmitoylation enhances T-cell immune responses against tumours. Nature Biomedical Engineering. 2019;3(4):306-17.
26. Abrami L, Kunz B, Iacovache I, Van Der Goot FG. Palmitoylation and ubiquitination regulate exit of the Wnt signaling protein LRP6 from the endoplasmic reticulum. 2008;105(14):5384-9.
27. Ernst AM, Syed SA, Zaki O, Bottanelli F, Zheng H, Hacke M, et al. S-palmitoylation sorts membrane cargo for anterograde transport in the Golgi. Developmental cell. 2018;47(4):479-93. e7.
28. Li Y, Martin BR, Cravatt BF, Hofmann SL. DHHC5 protein palmitoylates flotillin-2 and is rapidly degraded on induction of neuronal differentiation in cultured cells. Journal of Biological Chemistry. 2012;287(1):523-30.
29. Chen X, Niu W, Fan X, Yang H, Zhao C, Fan J, et al. Oct4A palmitoylation modulates tumorigenicity and stemness in human glioblastoma cells. Neuro-Oncology. 2022;25(1):82-96.
30. Chen X, Ma H, Wang Z, Zhang S, Yang H, Fang Z. EZH2 palmitoylation mediated by ZDHHC5 in p53-mutant glioma drives malignant development and progression. Cancer research. 2017;77(18):4998-5010.
31. Taftaf R, Liu X, Singh S, Jia Y, Dashzeveg NK, Hoffmann AD, et al. ICAM1 initiates CTC cluster formation and trans-endothelial migration in lung metastasis of breast cancer. Nature communications. 2021;12(1):4867.
32. Yao H, Lan J, Li C, Shi H, Brosseau J-P, Wang H, et al. Inhibiting PD-L1 palmitoylation enhances T-cell immune responses against tumours. Nature biomedical engineering. 2019;3(4):306-17.
33. Kurrikoff K, Langel Ü. Recent CPP-based applications in medicine. Expert Opinion on Drug Delivery. 2019;16(11):1183-91.
34. Kwon H, Choi M, Ahn Y, Jang D, Pak Y. Flotillin-1 palmitoylation turnover by APT-1 and ZDHHC-19 promotes cervical cancer progression by suppressing IGF-1 receptor desensitization and proteostasis. Cancer Gene Therapy. 2023;30(2):302-12.
35. Wang Y, Zhang S, He H, Luo H, Xia Y, Jiang Y, et al. Repositioning Lomitapide to block ZDHHC5-dependant palmitoylation on SSTR5 leads to anti-proliferation effect in preclinical pancreatic cancer models. Cell Death Discovery. 2023;9(1):60.
36. Lin CC, Lo MC, Moody RR, Stevers NO, Tinsley SL, Sun D. Doxycycline targets aldehyde dehydrogenase-positive breast cancer stem cells. Oncology reports. 2018;39(6):3041-7.

Figures

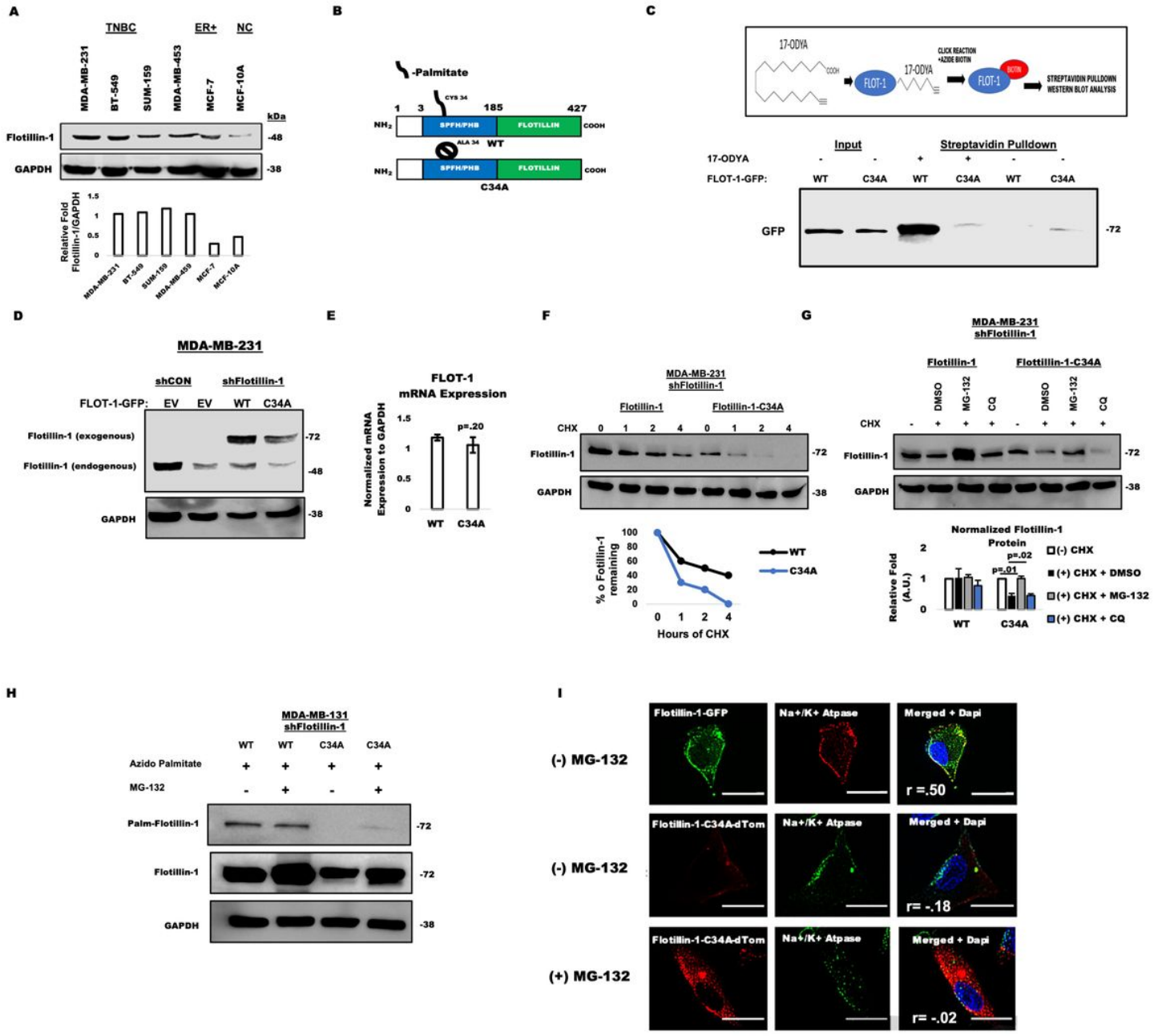

Figure 1

Palmitoylation-defective flotillin-1 displays altered stability and localization in TNBC cell lines. (A) Flotillin-1 protein expression in a panel of TNBC breast cancer cell lines as well as one (estrogen receptor +, ER+) MCF-7 and one non-cancerous (NC) MCF-10A cell line. The graph depicts band intensity of normalized flotillin-1 protein expression across the various cell lines. (B) Schematic representation of wildtype (WT) and cysteine-34-alanine (C34A) constructs. (C) Graphic depicting method of detecting palmitoylated flotillin-1 through click chemistry. Click chemistry analysis of the WT and C34A flotillin-1 constructs expressed in HEK293T cells by detecting GFP expression in the pull-down fractions. (D) Flotillin-1 protein expression analysis in MDA-MB-231 cells upon expression of empty vector or different flotillin-1 GFP plasmids. (E) Flotillin-1 mRNA expression between WT or C34A expressing MDA-MB-231

cells. Flotillin-1 expression was normalized to GAPDH mRNA and expressed as a fold change in the graph. The graph represents the mean three biological replicates (n=3) ± SD. (F) Flotillin-1 protein stability CHX chase assay in MDA-MB-231 WT and C34A flotillin-1 cells. Representative graph contains percentage of remaining flotillin-WT or C34A protein calculated by flotillin-1 protein band intensity normalize to GAPDH. The percentage of flotillin-1 remaining was calculated by dividing the normalized band intensity by the zero CHX condition to create a fold change and then multiplying by 100. This experiment was repeated twice with similar results. (G) Flotillin-1 wildtype or C34A expressing MDA-MB-231 cells were subjected to western blotting after the indicated treatments. The graph represents mean ± SEM from the quantification of flotillin-1 protein normalized to housekeeping protein from two independent trials. (H) Stably expressing flotillin-1 WT or C34A cells were treated with or without MG-132 were subjected to copper-free click chemistry to detect for palmitoylated flotillin-1 by western blotting. (I) Flotillin-1 GFP or Flotillin-1-C34A-dTomato MDA-MB-231 cells were subjected to immunofluorescence with an Na+/K+ ATPase antibody with either FITC or Cy3 secondary antibodies to detect membrane co-localization. Nuclei were stained with DAPI. Flotillin-1 C34A-dTomato expression was restored by treatment with 20 mM MG-132 for 8 hours. Colocalization between Na+/Kt ATPase and flotillin-1 was done in Image J using Pearson correlation coefficient expressed in the bottom left of the merged images denoted as “r=”.

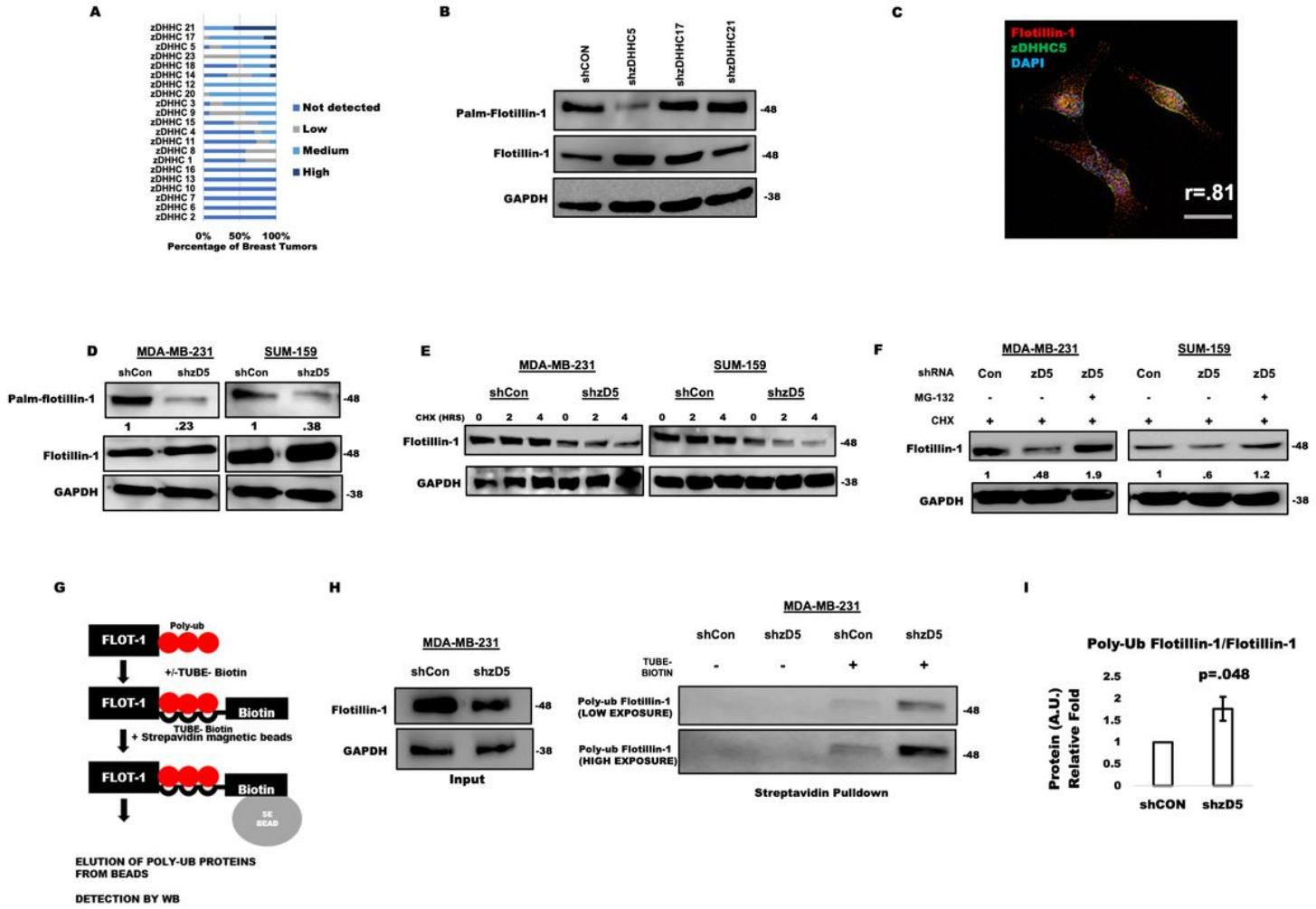

Figure 2

zDHHC5 contributes to the stability of endogenous flotillin-1 by preventing its proteasomal degradation. (A) Protein expression levels of zDHHC PAT enzymes in breast tumor samples assessed by IHC were obtained from the human protein atlas. (B) Stable shRNA expressing MDA-MB-231 cells against control, zDHHC 5, 17, and 21 were subjected to copper catalyzed click chemistry analysis to detect the palmitoylation status of endogenous flotillin-1 by western blotting. (C) Colocalization between endogenous flotillin-1 and zDHHC5 by immunofluorescent staining with flotillin-1 and zDHHC5 antibodies followed by Cy3 and FITC secondary antibodies, respectively. Nuclei were stained with DAPI. Colocalization is denoted as “r=” in the lower right corner which was obtained using the Image J coloc2 function (D) Flotillin-1 palmitoylation detection in Control shRNA (shCon) and zDHHC5 shRNA (shzD5)

stable MDA-MB-231 and SUM-159 cell lines using copper catalyzed click chemistry labeling followed by western blotting. (E) Flotillin-1 protein stability assessment in shCon vs shzD5 expressing MDA-MB-231 and SUM-159 cells using cycloheximide for the indicated time points. Flotillin-1 stability was assessed by western blotting with flotillin-1 antibody. (F) Flotillin-1 protein expression analysis in control (Con) or zDHHC5 (zD5) shRNA cells with or without CHX and MG-132. (G) Schematic representation of flotillin-1 poly-ubiquitin detection using biotin conjugated tandem ubiquitin binding entities (TUBEs). (H) Flotillin-1 poly-ubiquitylation was detected by a flotillin-1 antibody against the input and pulldown of the TUBE assay. (I) Quantification of the poly-ubiquitin state of flotillin-1 was quantified from the normalized band intensity from three biological replicates (n=3) between control (shCon) and zDHHC5 (shzD5) shRNA expressing MDA-MB-231 cells. Two-sided Students T-test was used for statistical analysis.

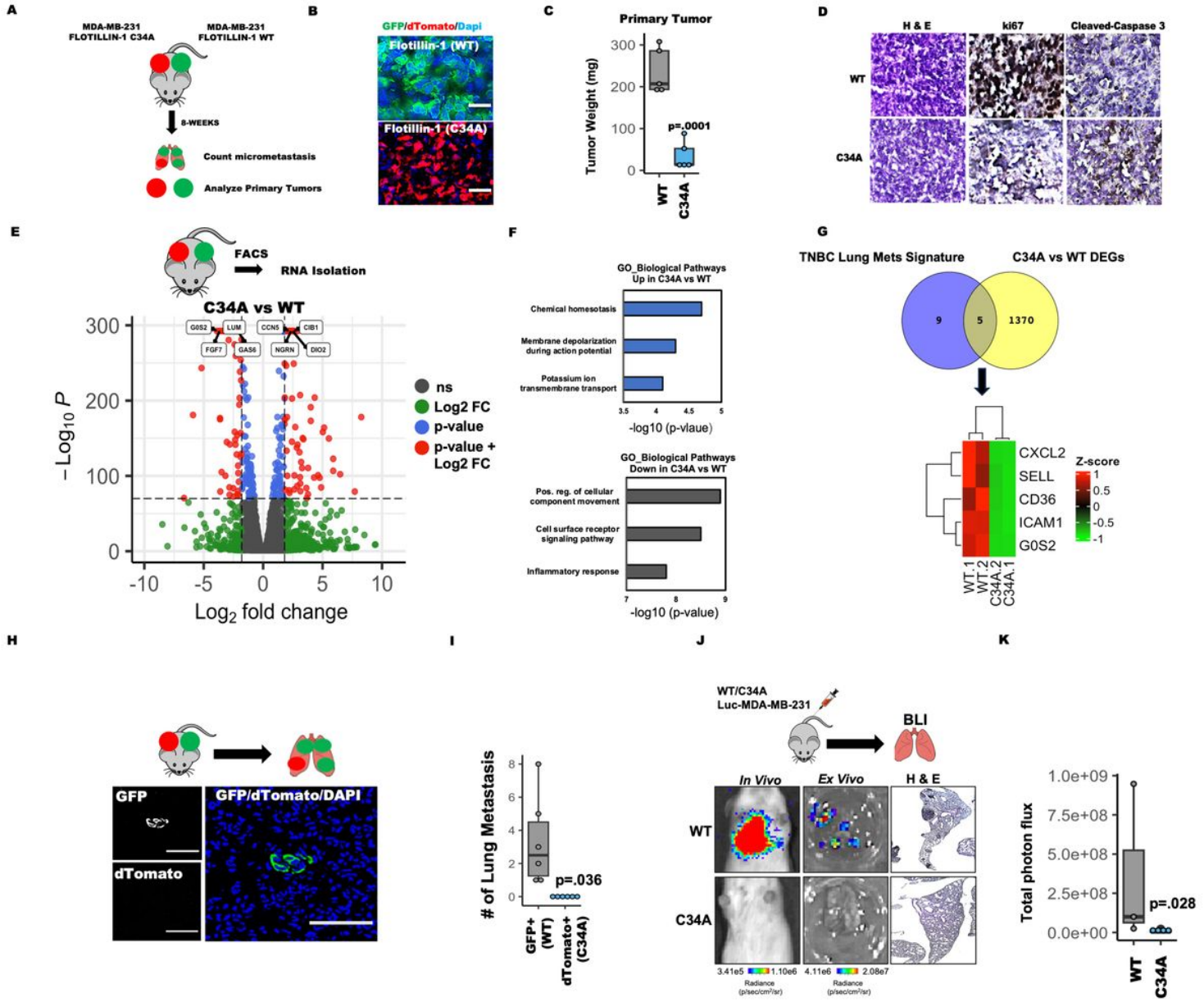

Figure 3

Flotillin-1 palmitoylation defective TNBC cells display attenuated tumor growth and lung metastasis. (A) Graphical representation of the spontaneous MDA-MB-231 xenograft metastasis model. (B) GFP and dTomato staining of WT and C34A flotillin-1 primary tumor sections with DAPI nuclei staining. (C) Box plot depicting the final primary tumor weight from (n=5) flotillin-1 wild type and C34A bearing tumors. Two-sided students T-test were performed for statistical analysis. (D) IHC analysis of tumor tissue sections from WT flotillin-1 and C34A flotillin-1 primary tumors. Sections were stained with H&E, Ki67, and cleaved caspase 3 that were counterstained with hematoxylin. (E) Bulk-RNA seq analysis using RNA isolated from FACS sorted GFP+ and dTomato+ tumors. Volcano plot represents up and down regulated genes in C34A expressing tumors vs WT. Color coding for the plot is listed to the right where “Log2 FC” stands for Log2 Fold Change in gene expression and “ns” stands for not-significant (F) Gene ontology biological pathway enrichment using the top upregulated and downregulated genes in C34A vs WT expressed by bar plot using normalized enrichment score (NES). (G) Differentially expressed genes (DEGs) (absolute log2fold of 1.5 and p-adjusted value < .05) from C34A vs WT RNA-seq overlapped with a 14 gene expression signature associated with TNBC lung metastasis. Significant overlapping genes were visualized by heatmap using normalized Z-score values. (H) Representative lung section image from lung metastasis generated from orthotopic tumors. Lung sections were stained with GFP or dTomato antibodies followed by FITC or Cy3 secondary antibodies. Nuclei were stained with DAPI. (I) Analysis of lung metastasis by counting the number green vs red cancer cells in lung sections from mice (n=5) after immunostaining. At least 3-4 slides per lung was used for the quantification of all five mice. Students two-side T-Test was performed for statistical analysis of the number of green vs red metastatic cells counted in each lung. (J) Representative IVIS images from whole mice or lungs harboring WT and C34A flotillin-1 expressing MDA-MB-231 cells. Confirmation of metastasis by performing H&E staining on fixed lung sections from mice. (K) BLI quantification from *ex vivo* lungs 28 days after intravenous lateral tail vein injection (3 WT and 4 C34A mice). The graph was constructed from the total photon flux of the lungs *ex vivo*. Box plot representing total photon flux of WT and C34A lungs. Mann-Whitney *U*-test was used for statistical analysis.

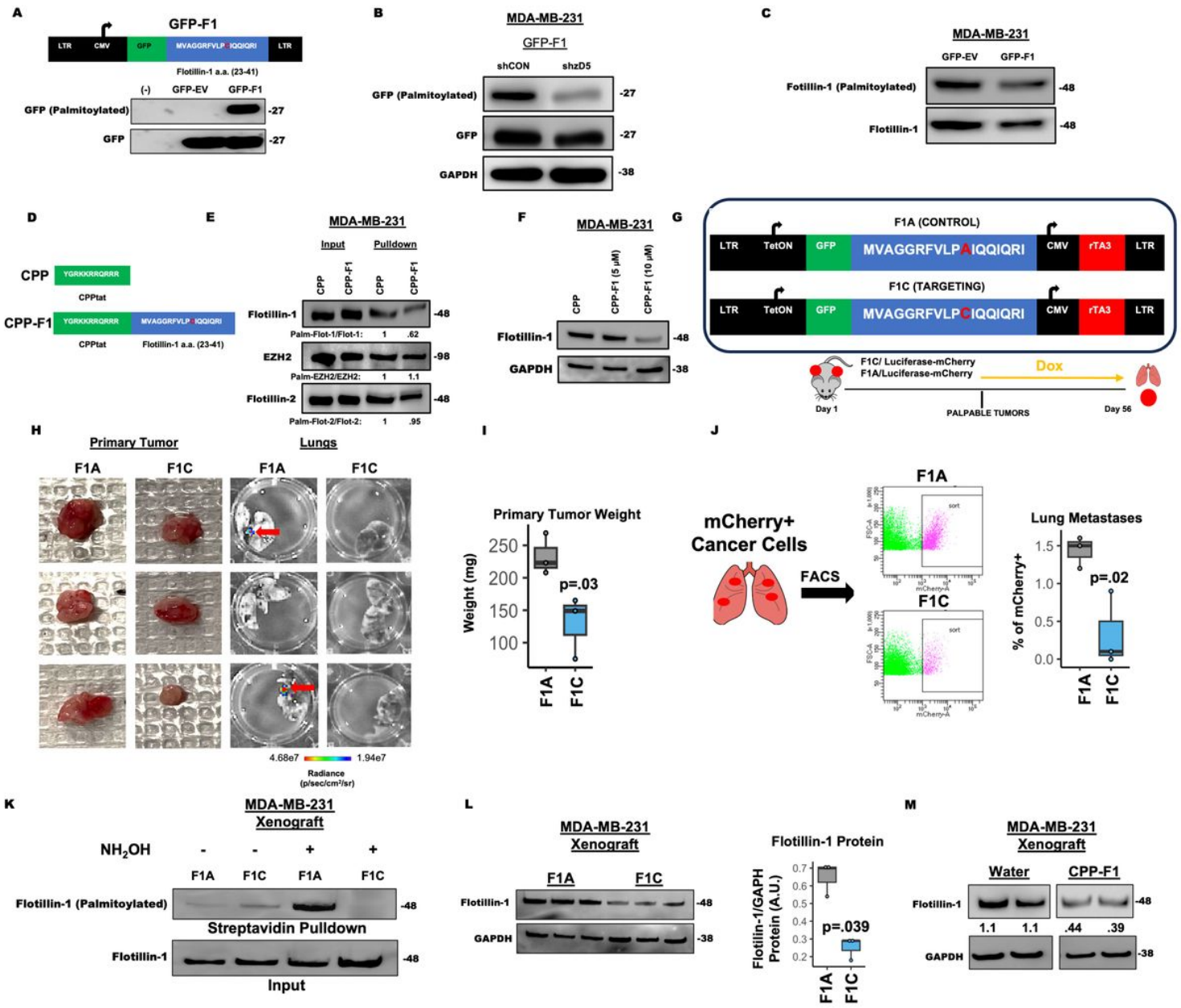

Figure 4

Targeting flotillin-1 palmitoylation with a competitive peptide attenuates tumor growth and lung metastasis. (A) Schematic and cloning strategy to create the GFP-flotillin-1 peptide construct. Analysis of GFP-F1 peptide palmitoylation by click chemistry. MDA-MB-231 cells alone, stable empty backbone GFP vector (GFP-EV), or GFP-F1 peptide (GFP-F1) were treated with 25 mM of 17-ODYA followed by copper catalyzed click chemistry detection. GFP palmitoylation was detected by western blotting with a GFP antibody of the streptavidin pulldowns. (B) The GFP-F1 construct was expressed in stable control or zDHHC5 shRNA MDA-MB-231 cells and subjected to copper catalyzed click chemistry detection. GFP palmitoylation was detected by GFP antibody of the streptavidin pulldown. (C) Endogenous flotillin-1 palmitoylation detection in MDA-MB-231 cells expressing empty vector GFP (GFP-EV) or GFP-F1 peptide.

(D) Schematic representation of peptides. The CPPtat sequence alone was used as a control compared to CPPtat fused to a flotillin-1 targeting peptide sequence. (E) TNBC cell lines were treated with 10 μM of CPPtat alone (CPP) or 10 μM of CPPtat fused to flotillin-1 targeting peptides (CPP-F1) for 24 hours. Flotillin-1, EZH2, and follillin-2 protein were detected by western blotting. (F) Flotillin-1 protein expression after 24 hours of 10 μM CPP, 5 μM, or 10 μM CPP-F1. (G) Schematic representation of xenograft model with tumors haboring doxycycline inducible peptide constructs along with mCherry-luciferase reporters. (H) Representative images from from MDA-MB-231 xenografted tumors along with *ex vivo* BLI images of lungs. (I) Box plot depicting the final tumor weight from the MDA-MB-231 xenograft (n=3) Students T-test was performed for statistical analysis (J) Box plot demonstrating the percentage of mCherry+ cancer cells detected from single cell suspensions generated from the lungs of mice harboring xenografted tumors (n=3). Students T-test was performed for statistical analysis. (K) Flotillin-1 palmitoylation detection by acyl-biotin exchange from xenografted primary tumors. -NH_2OH (hydroxylamine) represents the experimental negative control. This analysis was done with pooled samples from three F1A and F1C primary tumors. (L) Flotillin-1 protein expression from F1A and F1C expressing tumors. Representative box plot is a normalized flotillin-1 protein expression (to GAPDH) from F1A vs F1C tumors (n=3). Students T-test was performed for statistical analysis. (M) Mice harboring MDA-MB-231 xenografted tumors were treated by I.P. injection with either water only (water) or 150 ug of CPP-F1 peptide dissolved in water (CPP-F1) for 24 hours. Flotillin-1 protein was detected from two water and two CPP-F1 peptide treated tumors (n=2). Band intensity is represented below the membrane and was calculated by normalizing flotillin-1 intensity to GAPDH.

Supplementary Files

This is a list of supplementary files associated with this preprint. Click to download.

- SupplementaryMaterialsTable1.xlsx
- SourceDataAim2.xlsx
- SupplementalFigure1.jpg
- SupplementaryFigure2.jpg
- SupplementaryFigure3.jpg
- SupplementaryFigure4.jpg
- SupplementaryFigure5.jpg
- supplementaryfile6.jpg
- Supplementarydataandmethods.docx